ANZIAM J. **68, e20** (2026), 1–26
doi:10.1017/S1446181126100431

THE NOT-SO-SIMPLE LINEAR STABILITY OF A PLANE STOKES LAYER

ANDREW P. BASSOM[1,†] and CHRISTIAN THOMAS[2]

(Received 19 May, 2026 UTC; accepted 18 June, 2026 UTC)

Abstract

Time-periodic flows play important roles in many practical problems, with a wide range of examples occurring in engineering, physiology and ocean dynamics, among others fields. While the stability of spatially developing fluid flows is a relatively well-studied topic of research, there is a relative paucity of corresponding results that discuss purely time-periodic flows. Here we examine the stability of the classical plane Stokes layer: this is the flow generated in a layer of fluid that lies above a bounding plate that oscillates harmonically in its own plane. It has proved surprisingly difficult to understand the linear stability of this type of fluid flow, and here we trace the steps that have been taken to achieve this goal. There is a significant difference between the theoretical description of the stability of a Stokes layer and the corresponding practical measurements. We discuss possible reasons for this discrepancy and its possible implications for more general time-periodic motions.

2020 *Mathematics subject classification*: 76M45.

Keywords and phrases: Perturbation series, asymptotic methods, viscous fluid flow, numerical methods, spectral methods.

1. Introduction

The topic of hydrodynamic stability is one that can trace its origins back to the middle of the nineteenth century. It finds application in a diverse range of fields, including aerodynamics, oceanography and astrophysics. At the heart of the problem is that

† This is a contribution to the series of invited papers by past ANZIAM medallists (Editorial, Issue 52(1)). Andrew P. Bassom was awarded the 2025 ANZIAM medal.

[1]School of Natural Sciences, University of Tasmania, Physics Building, PO Box 807, Sandy Bay, TAS 7006, Australia; e-mail: andrew.bassom@utas.edu.au
[2]School of Mathematical and Physical Sciences, Macquarie University, NSW 2109, Australia; e-mail: christian.thomas@mq.edu.au

© The Author(s), 2026. Published by Cambridge University Press on behalf of The Australian Mathematical Publishing Association Inc. This is an Open Access article, distributed under the terms of the Creative Commons Attribution licence (https://creativecommons.org/licenses/by/4.0), which permits unrestricted re-use, distribution and reproduction, provided the original article is properly cited.

Downloaded from https://www.cambridge.org/core. UNIVERSIDAD AUTONOMA METROPOLITANA, on 17 Nov 2026 at 23:50:36, subject to the Cambridge Core terms of use, available at https://www.cambridge.org/core/terms. https://doi.org/10.1017/S1446181126100431

although the governing equations of motion can admit solutions that correspond to a simple flow, such solutions are relatively rarely observed in practice. Although these flows represent mathematically acceptable solutions to the problem specified, the presence of instability can cause the flow to adopt a more complicated and intricate structure that is often turbulent. This then sets the scene for the central issue for hydrodynamic stability: can we predict the circumstances under which a flow might become unstable?

It is worth pointing out at the outset that many important texts have been devoted to the topic of fluid stability; we mention the books by Drazin and Reid [16] and by Criminale et al. [13] as just a couple of excellent examples. These contain extended discussions of the stability of classical viscous flows, such as Poiseuille and Couette flow through a channel. Other important classes of problems involve centrifugal motions and geophysical flows. In this, largely a review, paper, we shall not discuss any of these, but instead focus on the conceptually simple flow induced by small in-plane oscillations of a flat plate above which lies a deep layer of incompressible viscous fluid.

Unsteady flows occur naturally, with applications ranging from engineering to physiology. There are several articles that focus on the stability of flows composed partly of a steady component plus an oscillatory component with zero temporal mean [11]. In such flows, instability can be associated with the mean component, so that the stability properties of the flow may be ascertained by a perturbation-type analysis about the mean. When the flow is purely oscillatory, this approach is not possible, and an alternative strategy is required. In that vein, we consider the classical plane Stokes layer that is generated when an infinite rigid plate oscillates in its own plane with a velocity $U_0 \cos \omega t$. Above the plate sits an infinite viscous fluid of kinematic viscosity ν, and the movement of the bounding surface induces a flow which has a boundary-layer thickness $\delta \sim O(\sqrt{2\nu/\omega})$. A Reynolds number R can now be defined as

$$R = U_0/\sqrt{2\nu\omega}.$$

As the basic flow is $2\pi/\omega$-periodic in time, Floquet theory suggests that small disturbances to the flow have the form $\exp(\mu^* t)f$ plus its complex conjugate; here f is a function of the independent variables, which is also $2\pi/\omega$-periodic in time. Any growth or decay in the disturbance over a period can be subsumed within the Floquet exponent μ^*.

The first attempt to use this approach for the linear stability of the classical plane Stokes layer was made by Hall [20]. His results detected no evidence of instability for R smaller than about 160. Earlier numerical work by von Kerczek and Davis [47] had looked at the related problem in which a stationary upper boundary is placed within the fluid; then no instability could be detected for R up to about 400. Later numerical simulations [2] were unable to find any growing Floquet modes for values of R up to at least 500.

Many studies of disturbances introduced into a Stokes layer have shown that they evolve in a highly nonuniform way; this means that, over the course of a period,

Downloaded from https://www.cambridge.org/core. UNIVERSIDAD AUTONOMA METROPOLITANA, on 17 Nov 2026 at 23:50:36, subject to the Cambridge Core terms of use, available at https://www.cambridge.org/core/terms. https://doi.org/10.1017/S1446181126100431

a perturbation typically undergoes intervals of rapid amplification interspersed with times of correspondingly quick decay. This behaviour has prompted instability studies based on a so-called quasi-steady theory [24]. Quasi-steady theories can be split into one of essentially two classes. In the first of these, no assumption is made regarding the size of R, which is retained in the important governing equations [25]. In the second type of approach, we suppose that $R \to \infty$; Cowley [12] used this idea, coupled with a multiple scales type analysis, to show that for sufficiently large R there are times within the period during which disturbances can grow significantly. Later work [48] explored the weakly nonlinear development of high-frequency modes around times when they are instantaneously neutrally stable. Unfortunately, it has proved impossible to develop a quasi-steady analysis that tracks the evolution of a disturbance over the whole period of oscillation. It should be noted that De Souza [15] successfully demonstrated that quasi-steady theory can describe the large R limit of Floquet theory if the mean part of the basic flow is sufficiently large. In the case of the Stokes layer with precisely zero mean flow, these arguments no longer hold.

While many of these calculations relate to oscillatory flows over an infinite flat plate, most experiments are carried out in circular pipes; it needs to be appreciated that high frequencies of oscillation, or very large-diameter pipes, are needed just to obtain a reasonable approximation to the plane Stokes layer. Moreover, there are various ways to generate the flow; two frequently used configurations require that either the pipe itself is forced to oscillate [11] or else the fluid can be driven by a piston while the pipe is held stationary (see [1, 17, 22]). While these differences should not affect any stability predictions, they do alter the corresponding eigenfunctions and hence how any disturbances might be described. It should be appreciated that these various experiments have suggested a range of critical values of $R = R_c$ at which instability is observed to set in. There is a significant disparity in the size of R_c as measured by different experimental set-ups, although Hino et al. [22] have postulated that, when all taken together, the available evidence suggests that perhaps $R_c \approx 275$. That being said, all the predictions of R_c lie within parameter regimes at which the earlier theoretical analyses could not detect any evidence of instability at all.

This raises two obvious questions. Why is straightforward linear theory seemingly unable to predict instability when R is clearly greater than the critical values R_c suggested in experiments? Why are the various laboratory apparatuses unable to agree on a consistent transition value of R_c? These issues prompted a series of investigations aimed at probing more deeply the stability characteristics of the classical Stokes layer.

2. The governing equations

We consider the motion induced in a semi-infinite layer of viscous fluid by a flat plate located at $y = 0$, which undergoes in-plane oscillations. This movement occurs in the x-direction with a plate velocity $U_0 \cos \omega t$. If all lengths are scaled on $\sqrt{2\nu/\omega}$, velocities on U_0, and the dimensionless time $\tau = \omega t$ is introduced, then, in the absence

Downloaded from https://www.cambridge.org/core. UNIVERSIDAD AUTONOMA METROPOLITANA, on 17 Nov 2026 at 23:50:36, subject to the Cambridge Core terms of use, available at https://www.cambridge.org/core/terms. https://doi.org/10.1017/S1446181126100431

of disturbances, the classical Stokes layer flow is simply given by

$$u = U_B(y,\tau) = \exp(-y)\cos(y-\tau), \quad v = 0, \tag{2.1}$$

where u and v denote the flow velocities in the x- and y-directions, respectively.

The linear stability of (2.1) is found by imposing a disturbance of the form

$$(u,v) = (U_B,0) + \varepsilon\left(\frac{\partial\Psi}{\partial y}, -\frac{\partial\Psi}{\partial x}\right),$$

where $\varepsilon \ll 1$ and $\Psi(x,y,\tau)$ is an appropriate disturbance stream function. It is most convenient to decompose

$$\Psi(x,y,\tau) = \exp(iax)\exp(\mu\tau)\psi(y;\tau) + \text{complex conjugate}, \tag{2.2a}$$

where we point out that the disturbance wave number $a \in \mathbb{R}$ is supposed to be specified. We can then appeal to Floquet theory, which is concerned with the solution of differential equations with coefficients that are periodic functions of the independent variable. The key result for our purposes is that the (y,τ)-dependence of the solution can be written $\exp(\mu\tau)\psi(y;\tau)$, where $\psi(y;\tau)$ is 2π-periodic (in τ). Any exponential growth or decay in Ψ can be incorporated within the (complex-valued) Floquet exponent μ. Given this form for the disturbance stream function $\Psi(x,y,\tau)$, the associated perturbation vorticity is written in the form

$$Z = \exp(iax)\exp(\mu\tau)\zeta(y;\tau) + \text{complex conjugate}. \tag{2.2b}$$

We note that this stability formulation has been limited to consideration of two-dimensional modes that depend only on the x- and y-coordinates. This is justifiable because this problem is an example of a famous result known as Squire's theorem [34]. In its simplest form, this states that for a parallel shear flow of an incompressible fluid, two-dimensional perturbations become unstable at a lower R than do their three-dimensional counterparts. The upshot is that the stability of the plane Stokes layer can be deduced by restricting ourselves to purely two-dimensional modes, safe in the knowledge that if all two-dimensional disturbances are stable, then necessarily so are all three-dimensional ones. In passing, we remark that a slightly more complicated oscillatory profile can be generated if orthogonal, isochronous oscillations, again in the plane of the plate, are superimposed on the basic boundary motion. Provided the two perpendicular oscillations are out of phase with each other, the plate will undergo an orbital motion and the fluid velocity will be just the linear superposition of the Stokes-layer profiles corresponding to each direction of oscillation. Even with this more intricate motion, it can be shown that Squire's theorem continues to hold [7].

With these expressions noted, the governing stream function/vorticity equations, when linearized in ε, become

$$\frac{\partial\zeta}{\partial\tau} = \frac{1}{2}\left(\frac{\partial^2}{\partial y^2} - a^2\right)\zeta - \mu\zeta - iaRU_B\zeta + iaRU_{Byy}\psi\,, \tag{2.3a}$$

Downloaded from https://www.cambridge.org/core. UNIVERSIDAD AUTONOMA METROPOLITANA, on 17 Nov 2026 at 23:50:36, subject to the Cambridge Core terms of use, available at https://www.cambridge.org/core/terms. https://doi.org/10.1017/S1446181126100431

$$\zeta = \left(\frac{\partial^2}{\partial y^2} - a^2\right)\psi; \tag{2.3b}$$

this system needs to be solved subject to

$$\psi = \psi_y = 0 \text{ on } y = 0; \quad \psi, \zeta \to \infty \text{ as } y \to \infty. \tag{2.3c}$$

We have already remarked that the Floquet exponent $\mu \in \mathbb{C}$ and if we write

$$\mu := \mu_r + \mathrm{i}\,\mu_i\,,$$

where μ_r is the growth rate, we notice that the decomposition (2.2a) does not tie down the value of μ completely. It is clear that μ_i is only determined modulo unity because if we change this quantity by some integer $q \in \mathbb{Z}$ then we can still write the perturbation quantities in the forms (2.2a) with $\psi(y;\tau)$ and $\zeta(y;\tau)$ periodic. Thus, for definiteness, μ_i can be restricted to the range $-1/2 < \mu_i \leq 1/2$. However, this constraint can be tightened further. The governing equations also have the property that if μ, $\zeta(y;\tau)$ is a solution, then so is $\widetilde{\mu}, \widetilde{\zeta}(y;\tau+\pi)$. The consequence is that both left- and right-propagating waves with the same growth rate are possible. The upshot is that the range for μ_i can be confined to the interval $0 \leq \mu_i \leq 1/2$.

To solve the problem (2.3a), the variables are written in harmonics

$$(\psi, \zeta) = \sum_{n=-\infty}^{\infty} (\psi_n(y), \zeta_n(y)) \exp(in\tau).$$

Equating the coefficients of the harmonics within equations (2.3a) and (2.3b) leads to the system of coupled equations

$$\left(\frac{d^2}{dy^2} - a^2 - 2\mu - 2in\right)\zeta_n = iaR[\{\zeta_{n-1} - 2i\psi_{n-1}\}\mathrm{e}^{-(1+i)y} + \{\zeta_{n+1} + 2i\psi_{n+1}\}\mathrm{e}^{-(1-i)y}]$$

and

$$\left(\frac{d^2}{dy^2} - a^2\right)\psi_n = \zeta_n.$$

It was noted by Seminara and Hall [33] and Hall [20] that a semi-analytical solution of this problem is feasible. It may be shown that it is possible to write

$$\psi_n = \sum_{k=-\infty}^{\infty} \left\{\alpha_k \sum_{j=0}^{\infty} A_{jkn} E_{jkn}(\gamma_k) + \beta_k \sum_{j=0}^{\infty} B_{jkn} E_{jkn}(a)\right\}; \tag{2.4a}$$

here the constants

$$\gamma_k := \sqrt{a^2 + 2\mu + 2ik} \tag{2.4b}$$

and the exponential functions are defined by

$$E_{jkn}(\bullet) := \exp\{-[\bullet - i(k-n) + |k-n| + 2j]y\}, \tag{2.4c}$$

Downloaded from https://www.cambridge.org/core. UNIVERSIDAD AUTONOMA METROPOLITANA, on 17 Nov 2026 at 23:50:36, subject to the Cambridge Core terms of use, available at https://www.cambridge.org/core/terms. https://doi.org/10.1017/S1446181126100431

while the α_k and β_k remain arbitrary for the moment. Finally, we note that the coefficients A_{jkn} and B_{jkn} satisfy rather complicated recurrence relations. In the interests of brevity, we do not set out these relations here and the interested reader could consult [5] or [20] for full details. Now, provided that the real part of each γ_k is positive, the far-field $y \to \infty$ elements of the boundary conditions (2.3c) are automatically satisfied. Thus, we only need to ensure that the wall conditions $\psi = \psi_y = 0$ hold, which means that

$$\sum_{k=-\infty}^{\infty} \left\{ \alpha_k \sum_{j=0}^{\infty} A_{jkn} + \beta_k \sum_{j=0}^{\infty} B_{jkn} \right\} = 0 \tag{2.5a}$$

and

$$\sum_{k=-\infty}^{\infty} \left\{ \alpha_k \sum_{j=0}^{\infty} A_{jkn}[\gamma_k - i(k-n) + |k-n| + 2j] + \beta_k \sum_{j=0}^{\infty} B_{jkn}[a - i(k-n) + |k-n| + 2j] \right\} = 0. \tag{2.5b}$$

The infinite-dimensional system of equations (2.5a) can be cast as

$$\mathbf{M}\,\mathbf{v} = \mathbf{0}, \tag{2.6}$$

where $\mathbf{v}$ is a column vector consisting of the elements $\{\alpha_k, \beta_k\}$ with $-\infty < k < \infty$. A nontrivial solution for the vector $\mathbf{v}$ is required so that the determinant of the matrix $\mathbf{M}$ must vanish. This should yield the form of μ as a function of a and R.

3. The structure of the neutral curve

A numerical solution to the problem requires a good approximation to the full infinite-dimensional system (2.6). This was done by noting that since the $\psi_n(y)$ are the Fourier coefficients of a smooth periodic function, we expect that they rapidly tend to zero as $n \to \infty$. Accordingly, we truncate the system and assume that $\psi_m \equiv 0$ for $|m| \geq N + 1$. This leaves a system of $4N + 2$ equations for the unknowns α_r, β_s for $|r|, |s| \leq N$. Of course, it needs to be checked that N is chosen to be sufficiently large that the functions ψ_m with $|m| \geq N + 1$ are so small that the partial sum represents a sufficiently accurate approximation to the solution of the full system.

Hall [20] tackled this problem, but he could only find stable solutions ($\mu_r < 0$) for R up to about 160 and a truncation level of $N = 14$. It turns out that the required size of N tends to increase as R grows and the computer resources available at the time prevented Hall from taking his calculations to any greater R. It was only about a quarter of a century later that Blennerhassett and Bassom [5] revisited this problem. The intervening period of advances in technology, combined with the implementation of some judicious numerical strategies (see [5] for details), enabled the calculations of Hall to be extended to much higher values of R. Indeed, it proved possible to locate a

Downloaded from https://www.cambridge.org/core. UNIVERSIDAD AUTONOMA METROPOLITANA, on 17 Nov 2026 at 23:50:36, subject to the Cambridge Core terms of use, available at https://www.cambridge.org/core/terms. https://doi.org/10.1017/S1446181126100431

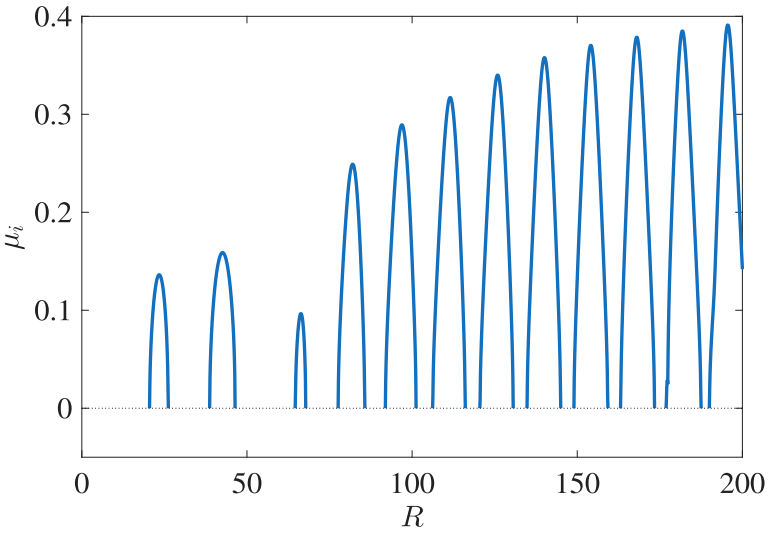


FIGURE 1. The imaginary part μ_i as a function of R for $a = 0.3$ and $R \leq 200$. The intervals between the solution branches are the S-gaps where there are no solutions that decay as $y \to \infty$.

portion of the neutral curve, with growing modes identified once R exceeds about 708. We describe these results below, but note here that the calculations typically required N to be at least 200, and sometimes more than that. This then requires that the zeros of an 800×800 determinant be located and special measures had to be taken to ensure numerical accuracy was preserved.

The variation of the imaginary part μ_i as a function of R up to about 200 and with a wave number $a = 0.3$ is shown in Figure 1. There are intervals of R where solutions exist; between these are regions across which no solutions appear to be possible. At the edges of these intervals $\mu_i \to 0$ and γ_0 is purely imaginary since $a^2 + 2\mu_r < 0$. Then the solution is only bounded at infinity rather than decaying in that limit. If these breaks in the solution branches are referred to as S-gaps, it appears that as R increases, the lengths of these gaps decrease. At the same time, the heights of the peaks in Figure 1 appear to grow towards the value 0.5. When $\mu_i \neq 0$, discrete eigenvalues correspond to travelling wave disturbances and, as will be explained presently, the S-gaps eventually evolve into standing wave modes.

When $a = 0.3$, the results suggest that the disturbance becomes neutrally stable, with $\mu_r = 0$ and $\mu_i \neq 0$ when $R \approx 780$. As a consequence, there is a range of R just below this neutral point where $a^2 + 2\mu_r$ is positive, and this has an important implication for the nature of the solutions in the S-gaps just below any such neutral points. (With $a = 0.3$, the relevant range is $772 \lesssim R \lesssim 780$.) The behaviour of the eigensolution at infinity is dictated by the nature of the $E_{000}(\gamma_0)$ term in (2.4c). At the edges of the S-gaps $\mu_i = 0$ but now, since $a^2 + 2\mu_r > 0$, solutions with a negative real part of γ_0 are possible. Hence, an eigenfunction that decays at infinity exists with

Downloaded from https://www.cambridge.org/core. UNIVERSIDAD AUTONOMA METROPOLITANA, on 17 Nov 2026 at 23:50:36, subject to the Cambridge Core terms of use, available at https://www.cambridge.org/core/terms. https://doi.org/10.1017/S1446181126100431

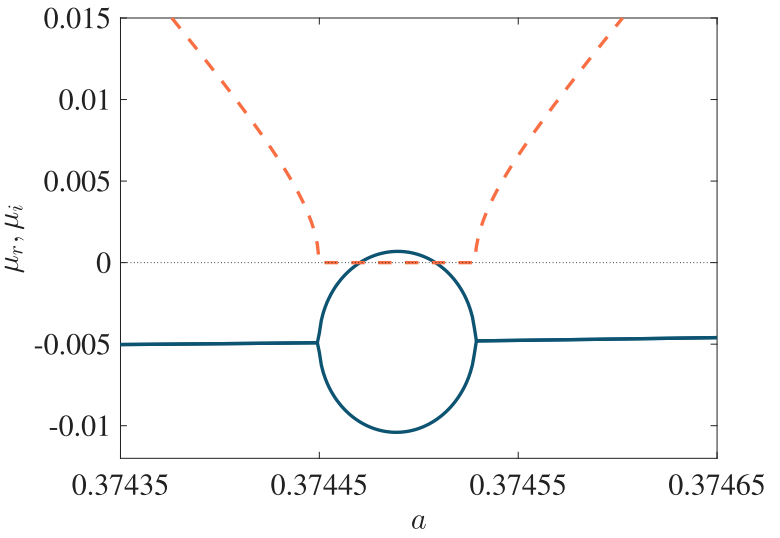


FIGURE 2. The real (μ_r; solid) and imaginary (μ_i; dashed) parts of the Floquet exponent μ as a function of a when $R = 708$. In the left and right portions of the range, where $\mu_i \neq 0$, the two travelling waves have identical growth rates μ_r (< 0). Across the middle section, where we have coalescence of the travelling waves, $\mu_i \equiv 0$ and the two standing waves have different growth rates. We also see that for a small range of a, one of these standing waves has $\mu_r > 0$ so is unstable.

$\mu_i = 0$; that is, it is a standing wave. We conclude that S-gaps at values R well below neutral conditions contain a continuous spectrum of standing wave modes which do not decay at infinity, since γ_0 is purely imaginary. By way of contrast, within S-gaps just below neutral conditions, there are discrete, standing wave disturbances that decay from the oscillating plate.

Some greater detail of the above structure is provided in Figure 2 for $R = 708$. Across the S-gap $\mu_i = 0$ but is nonzero on either side. Note that where μ is complex, only the eigenvalues with $\mu_i > 0$ have been plotted; the complex conjugate eigenvalues $\widetilde{\mu}$ have been omitted, so the behaviour of the growth rate can be seen more easily. The endpoints of these intervals clearly correspond to a coalescence of the left and right travelling wave modes, that is, a coming together of complex conjugate eigenvalues, and while μ_r is a continuous function of a, it must have square-root behaviour at the endpoints of the $\mu_i = 0$ interval. The most remarkable feature of the disturbance in this interval is that the two standing wave solutions, coming from the collision of the complex conjugate eigenvalues, have distinctly different growth rates. One of the modes is actually unstable on part of this S-gap. At the upper end of this interval, the standing wave modes are again both stable and they combine to give stable travelling wave modes as a is increased past the right-hand end of the S-gap. The existence of these regions of unstable stationary modes, just below the bulk of the unstable region of parameter space, made the precise determination of the neutral curve far from straightforward.

Downloaded from https://www.cambridge.org/core. UNIVERSIDAD AUTONOMA METROPOLITANA, on 17 Nov 2026 at 23:50:36, subject to the Cambridge Core terms of use, available at https://www.cambridge.org/core/terms. https://doi.org/10.1017/S1446181126100431

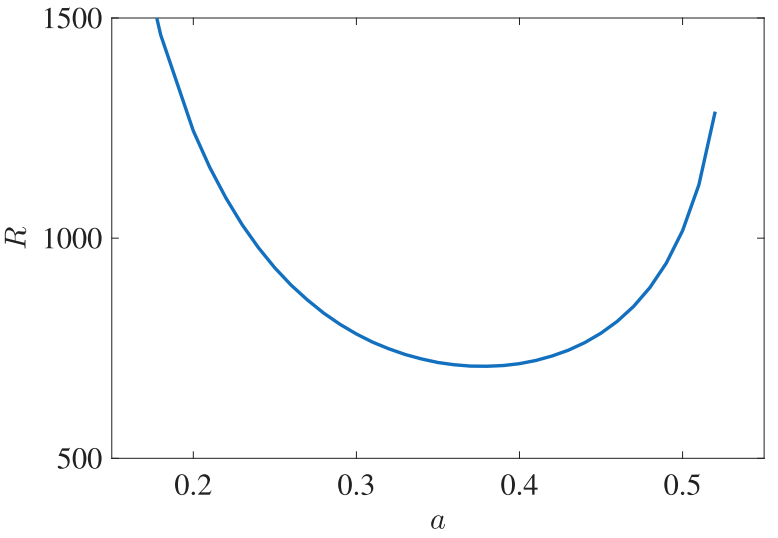


FIGURE 3. Smoothed neutral curve for linear instability in the (a, R)-plane. Modes in the parameter regime above the curve are linearly unstable.

Part of the neutral curve on which $\mu_r = 0$ is depicted in Figure 3. This curve was constructed by simple interpolation through neutral points separated in the wave-number domain by an increment of $\Delta a = 0.01$. However, the detailed structure of the curve is rather more intricate than is perhaps suggested by Figure 3. We have just noted that throughout the parameter space, there are short intervals where stationary modes exist with significantly different growth rates. What can happen is that if an interval of stationary modes lies below, but close to the smooth curve in Figure 3, then it is possible for one of the stationary modes to actually become unstable. The complete neutral curve can then only be ascertained by combining the form of the smooth neutral curve with the topology of the regions where stationary modes have $\mu_r = 0$.

The rather intricate composite curve near the wave number $a = 0.38$ is illustrated in Figure 4. The wavy upper section of the curve is a zoomed-in version of the global curve shown in Figure 3. On this section of the curve, the modes take the form of travelling waves with $\mu_i \neq 0$. However, we can see that the upper section is punctured by two thin "fingers"; these are stationary modes with $\mu_i = 0$. We can see that the critical disturbance (that is, the one that occurs at the smallest value $R = R_c$) is actually stationary; it has wave number $a \approx 0.3746$ with $R_c \approx 707.84$. It should be noted that, for this particular value of a, the stationary mode occurs at a lower R than does the corresponding travelling form. However, this only occurs occasionally and, for most wave numbers, it is the travelling mode that is the first to become unstable. The fingers seem to have a length of about 1 in R-space, so are relatively short. It should also be emphasized that the finger-like structures shown near the minimum of the critical

Downloaded from https://www.cambridge.org/core. UNIVERSIDAD AUTONOMA METROPOLITANA, on 17 Nov 2026 at 23:50:36, subject to the Cambridge Core terms of use, available at https://www.cambridge.org/core/terms. https://doi.org/10.1017/S1446181126100431

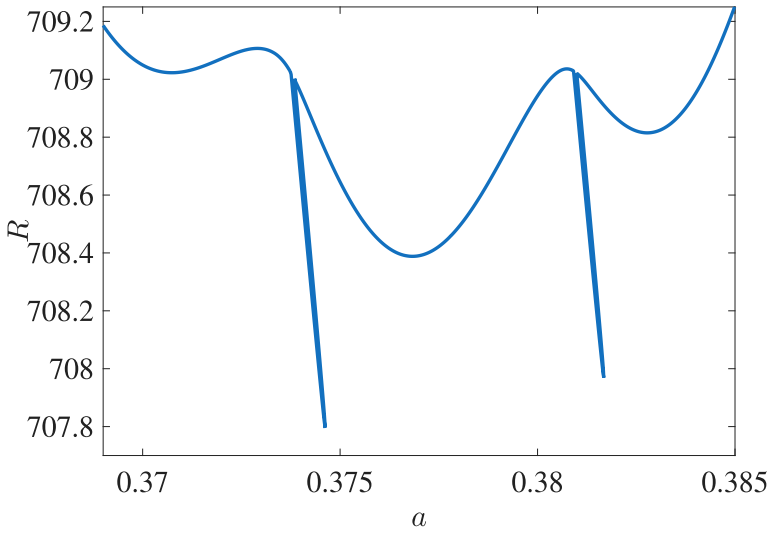


FIGURE 4. Detailed form of the neutral curve over the range $0.368 \leq a \leq 0.385$.

curve in Figure 4 are not restricted to this part of the curve. Strictly speaking, the smoothed form of the curve sketched in Figure 3 should be modified by stationary mode spikes that occur intermittently along the whole line. Significantly, these features are closely connected to the underlying nature of the instability and its spatio-temporal development, which we discuss further in Section 5.

We mentioned in the introduction that the associated experimental investigations have suggested that $R_c \approx 275$, which is considerably lower than the theoretical prediction based on Floquet theory. Several explanations might account for this discrepancy. One possibility is that although the curve sketched in Figures 3 and 4 constitutes one solution, there may be other neutral curves located elsewhere in the parameter space; however, extensive explorations by [5] failed to detect any. We also point out that experiments are necessarily conducted within a finite apparatus, in contrast to the infinite plane layer used in the theoretical analysis.

This latter point prompted [6] to investigate the stability of oscillatory flow in a finite channel. The flow configuration consists of two parallel plates separated by a distance $2d$ that oscillate synchronously with velocity $U_0 \cos \omega t$. If the dimensionless half-width of the channel is h, the modified form of the basic Stokes flow becomes

$$U_B(y,\tau) = \Re\left\{\frac{\cosh((1+i)y)}{\cosh((1+i))h)}\exp(i\tau)\right\} \equiv u_1(y)\exp(i\tau) + u_{-1}(y)\exp(-i\tau),$$

for $|y| \leq h$. The perturbation equations are again given by system (2.3a), albeit with the modified form of U_B and with the boundary conditions given by $\psi = \psi_y = 0$ when $y = \pm h$.

Downloaded from https://www.cambridge.org/core. UNIVERSIDAD AUTONOMA METROPOLITANA, on 17 Nov 2026 at 23:50:36, subject to the Cambridge Core terms of use, available at https://www.cambridge.org/core/terms. https://doi.org/10.1017/S1446181126100431

Once the perturbation equations apply over a finite domain, rather than on the semi-infinite region, the semi-analytical solution proposed in [20] is no longer available. Consequently, the calculations performed in [6] were based on pseudo-spectral techniques as derived and described by Fornberg [18] or Trefethen [44]. The computations revealed that now two families of solutions were feasible. The first, which we will refer to as a wall mode, is concentrated near one of the oscillating walls and is the natural counterpart of the disturbance within a semi-infinite layer. However, the finite geometry also introduces a second structure centred around the middle of the channel; this structure has no counterpart within the semi-infinite layer. Thorough investigations showed that these centre modes are always stable for all values of a and R, so can be safely ignored for the purposes of identifying when the underlying flow becomes unstable.

Blennerhassett and Bassom [6] could therefore focus on the wall modes and they monitored their properties as the channel width varied. As would be expected, when the channel is very wide, with $h \gtrapprox 16$, the stability characteristics are essentially identical to those of the semi-infinite layer with $R_c \approx 708$. As h is reduced, the value of R_c falls and appears to attain a minimum when $h \approx 5$, for which $R_c \approx 645$. While this is lower than the prediction for the semi-infinite problem, there remains a sizeable discrepancy with the experimental determinations of R_c. In an attempt to more faithfully replicate the practical apparatus, Blennerhassett and Bassom [6] extended their methods to account for perturbations to the Stokes layer that is established within a pipe oscillating along its axis. This basic flow can be expressed in terms of Bessel functions of order zero and the governing system for the disturbance needs to be adapted to properly account for the cylindrical geometry. The critical Reynolds number for pipe flow tends to be smaller than their counterparts for the channel case, but the smallest critical value was still almost twice the experimentally reported result.

The veracity of these various theoretical results based on Floquet theory has naturally been questioned, given the disparity with the carefully conducted experiments. In order to throw more light on this issue, Thomas et al. [38] conducted a series of direct numerical simulations based upon a velocity–vorticity formulation of the governing equations. This enabled the time evolution of disturbances to be tracked in an efficient way. In particular, it proved possible to locate the neutral stability curve for two-dimensional disturbances and this was found to be in excellent agreement with the outcomes of the Floquet studies. As a by-product, the two-dimensional neutral stability results were then used to validate the extension of the direct numerical solution code to describe three-dimensional disturbances that take the form of oblique waves.

The methods introduced in [38] were subsequently adapted in [39] to look at the stability of oscillatory Poiseuille flow in both channels and pipes. In these calculations, the underlying basic motion consists of a steady pressure-gradient-driven velocity field coupled with a purely oscillatory component generated either using an oscillatory pressure gradient or by harmonically oscillating the bounding surfaces. Both plane channel and circular pipe geometries were studied and neutral stability curves and critical conditions for instability computed for a selection of steady–unsteady velocity

Downloaded from https://www.cambridge.org/core. UNIVERSIDAD AUTONOMA METROPOLITANA, on 17 Nov 2026 at 23:50:36, subject to the Cambridge Core terms of use, available at https://www.cambridge.org/core/terms. https://doi.org/10.1017/S1446181126100431

ratios, channel half-widths and pipe radii. The results obtained again confirm previous investigations into the effects of small amounts of periodic modulation on the linear stability of the underlying steady flow, but provided much more comprehensive information on the linear stability regions of unsteady parallel flows in channels and pipes.

These numerical methods were extended by [37] to probe the three-dimensional linear stability of the Stokes layer generated within a fluid contained inside a long oscillating cylinder. Critical parameters for instability were obtained for an extensive range of pipe radii and longitudinal and azimuthal wave numbers. We noted earlier that Squire's theorem holds for an infinite plane Stokes layer, but the results established in [37] show that, for sufficiently small pipe diameters, three-dimensional perturbations are actually more unstable than their two-dimensional counterparts. By way of contrast, at larger radii, the three-dimensional disturbance modes are less important and the two-dimensional versions are dominant, so are expected to be observed in practice. These results have important implications for the constraints that should be imposed on experiments that are designed to exhibit shear modes in oscillatory flow.

4. The discrepancy between theory and experiment: a plausible explanation?

Thus far, we have seen that there remains a rather large difference in the critical conditions predicted by Floquet theory and those measured in the laboratory. In their calculations, Blennerhassett and Bassom [5] had noted that a neutral disturbance mode, though periodic over the course of one complete period $0 \leq \tau \leq 2\pi$, undergoes intervals of rapid growth (together with corresponding times of rapid decay). If we adopt the magnitude of the wall vorticity $\zeta_{\mathrm{w}} := |\zeta(0, \tau)|$ as an avatar for the size of the disturbance, then over the course of a cycle and with $R = 255$ (close to experimental conditions) the greatest value of ζ_{w} is about ten times its least. Once $R = 500$ this ratio becomes 40, and near the theoretical critical $R = 708$ it is almost 200. The implication is that if we allow for a maximum disturbance amplitude of 2% at critical conditions, the background noise in the wall vorticity would need to be less than about 0.01% if the predicted linear stability were to be observable experimentally. This requirement is unrealistically demanding; typical equipment, such as that described by Eckmann and Grotberg [17], reports noise levels of maybe a few per cent at best.

In an effort to assess the effect of noise on the stability of the plane Stokes layer, Thomas et al. [41] examined a generalisation of the problem of a Stokes layer between a pair of infinite flat plates separated by a dimensionless distance $2h$. As a paradigm for wall noise, the plate velocities U_w were set to be

$$U_w = U_0 \cos\tau + U_0\delta(\alpha_p \cos p\tau + \beta_p \sin p\tau) \quad \text{where } \alpha_p^2 + \beta_p^2 = 1; \tag{4.1}$$

here it has been supposed that the theoretical wall velocity $\cos\tau$ is perturbed by a second frequency p. This effect may be interpreted as a component of noise. The size of this noise is measured by δ, while its phase relative to the main oscillation is controlled by adjusting α_p and β_p as appropriate. Of course, in practical settings, the

Downloaded from https://www.cambridge.org/core. UNIVERSIDAD AUTONOMA METROPOLITANA, on 17 Nov 2026 at 23:50:36, subject to the Cambridge Core terms of use, available at https://www.cambridge.org/core/terms. https://doi.org/10.1017/S1446181126100431

noise would be expected to comprise a spectrum of frequencies, but for simplicity this model includes just one. The numerical calculations were conducted for noise levels up to about 3%.

With the wall velocity as specified by (4.1), the scaled basic velocity profile is given by

$$U_{Bn}(y,\tau) = \Re\left\{\frac{\cosh((1+i)y)}{\cosh((1+i)h)}\exp(i\tau) + \delta\frac{\cosh((1+i)y\sqrt{p})}{\cosh((1+i)h\sqrt{p})}(\alpha_p - i\beta_p)\exp(ip\tau)\right\}.$$

With this basic profile, the governing equation for the perturbation stream function ψ becomes

$$\frac{\partial}{\partial\tau}\mathcal{L}\psi = \left\{\frac{1}{2}\mathcal{L} - \mu - iaRU_{Bn}\right\}\mathcal{L}\psi + iaR\left(\frac{\partial^2 U_{Bn}}{\partial y^2}\right)\psi\,;$$

here we have introduced the linear operator

$$\mathcal{L} \equiv \frac{\partial^2}{\partial y^2} - a^2$$

and seek solutions with

$$\psi = \psi' = 0 \quad \text{on } y = \pm h.$$

Numerical solutions were generated by using a velocity–vorticity formulation based on the strategy proposed by Davies and Carpenter [14].

It is far from clear at the outset which values of the frequency p might prove to be significant. To ascertain the most likely candidates, a sensitivity analysis was conducted. This was done by linearising the problem in δ, whereupon we suppose that if

$$\psi(y,\tau) = \psi^{(0)}(y,\tau) + \delta\psi^{(1)}(y,\tau) + \cdots,$$

then the corresponding Floquet exponent $\mu = \mu^{(0)} + \delta\mu^{(1)} + \cdots$. The problem for $\psi^{(0)}$ replicates the eigenvalue problem solved in [6] and then the governing problem for $\psi^{(1)}$ is just a forced version of that for $\psi^{(0)}$. This can only admit a solution if a suitable solvability condition is satisfied, a constraint that can be derived using standard techniques based on the consideration of appropriate adjoint functions.

The outcome of this sensitivity analysis yielded the somewhat unexpected result that components of relatively high-frequency noise with p around 50–80 are those that have the most effect on the value of μ. This informed a subsequent set of calculations for finite δ. Some representative results are shown in Figure 5, where we illustrate the effect of increasing the size of δ on the real part of the growth rate μ_r for both the wall and the centre modes in channels of width 5 and 16 at a Reynolds number $R = 300$. In the narrower channel, the wall mode is always more unstable than the centre mode; moreover, a noise level of a mere 1% is sufficient to make the previously stable flow unstable. This can be deduced from Figure 5 where the blue line is seen to cross over into the unstable $\mu_r > 0$ region when $\delta \approx 2 \times 10^{-3}$. We emphasize that this small noise

Downloaded from https://www.cambridge.org/core. UNIVERSIDAD AUTONOMA METROPOLITANA, on 17 Nov 2026 at 23:50:36, subject to the Cambridge Core terms of use, available at https://www.cambridge.org/core/terms. https://doi.org/10.1017/S1446181126100431

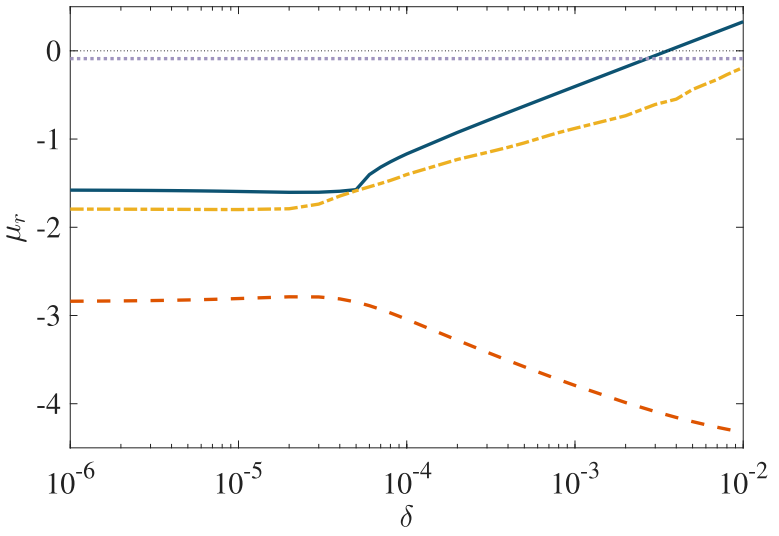


FIGURE 5. The real part of the Floquet exponent μ_r for the wall and centre modes when $R = 300$ as the noise level δ is increased. The solid and dashed lines show the results for the wall mode and centre mode, respectively, for the narrow channel $h = 5$; the wave number $a = 0.41$ and the noise frequency $p = 75$. The chain and dotted lines are the wide channel $h = 16$ counterparts with $a = 0.38$ and $p = 65$.

component is enough to drive the transition value of R to less than half its theoretical value for the basic flow in the absence of noise. We also comment that although a 1% noise level is insufficient to make the wide channel unstable, the decay rate of the wall mode is very close to zero, having more than halved.

Another perspective on the role of relatively high-frequency noise is provided in Figure 6. Here we illustrate the real part μ_r for a wave number $a = 0.41$ in a wide channel $h = 16$ with $R = 300$. We remark that the noise amplitude is fixed at 1% ($\delta = 0.01$) and the frequency range $50 \leq p \leq 100$ is considered. For p below 50, or above about 85, the eigenvalues obtained are essentially those that would be found for a noise-free, purely oscillatory flow and the results for the wall mode are not visible within the range of μ_r shown in the figure. Once p is above approximately 60, the wall mode begins to be substantially affected by the noise within the basic flow; μ_r starts to increase. The wall mode becomes more unstable than both the centre modes for $71 \leq p \leq 76$ while, as seen previously, the centre mode eigenvalues remain almost completely unaffected. Again, μ for the wall mode does not quite reach the right-hand half of the complex plane; it seen in Figure 6 that although the real part of μ stays negative, it attains a maximum value of about -0.02 when $p = 73$, which suggests that the flow is then only very weakly stable.

A global view of the effect of noise on the stability of the underlying oscillatory flow is provided by examining suitable neutral stability curves in the (a, R)-plane. Some examples of the neutral stability curves for the noisy flow are shown in Figure 7.

Downloaded from https://www.cambridge.org/core. UNIVERSIDAD AUTONOMA METROPOLITANA, on 17 Nov 2026 at 23:50:36, subject to the Cambridge Core terms of use, available at https://www.cambridge.org/core/terms. https://doi.org/10.1017/S1446181126100431

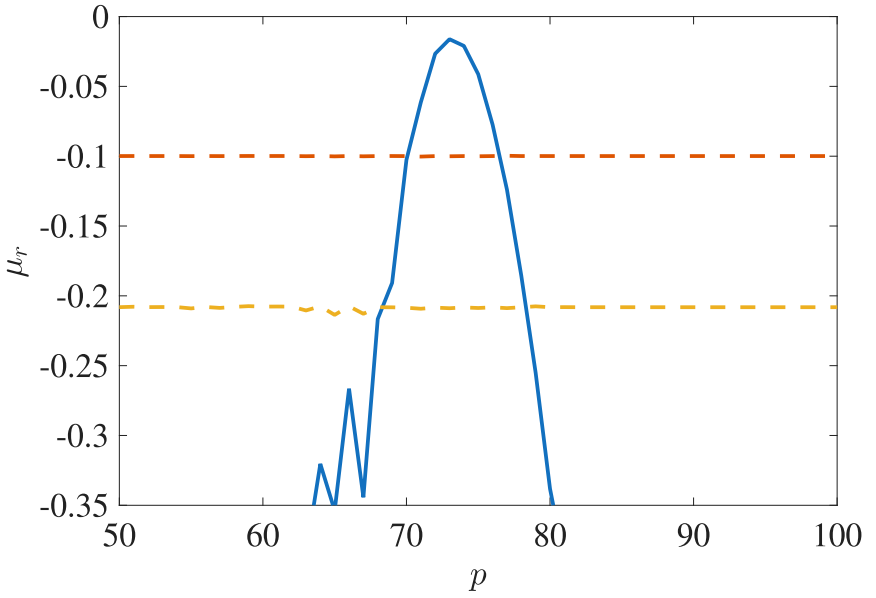


FIGURE 6. The real part of μ for the three most unstable modes as a function of noise frequency p when $h = 16, a = 0.41, \delta = 0.01$ and $R = 300$. The dashed and dotted lines correspond to the first two centre mode disturbances, while the solid line indicates the growth rate of the wall mode.

Three curves for the most unstable even mode disturbances are illustrated. Despite the slightly unusual shape of these neutral curves, the remarkable feature common to all of them is the surprisingly small value of the critical $R = R_c$. For the wide channel $h = 16$, the model of the semi-infinite Stokes layer, we see $R_c \approx 305$ for noise frequencies of both 69 and 76. This is a reduction of over 400 compared with its theoretical value of $R_c \approx 708$ for the single-frequency flow. We also note that while the neutral curves drawn in Figure 7 are explicitly for disturbances that exhibit even symmetry about the centre of the channel, the neutral curves for odd modes are graphically indistinguishable.

Superimposed on Figure 7 are the critical conditions (marked by + signs) obtained for a range of other frequencies when $\delta = 0.01$. At this noise level, when $p = 35$, the value of R_c is essentially unchanged from its size $R_c \approx 708$ in a noise-free environment. When $p \in [67, 81]$, we find that R_c remains fairly constant at roughly 305. It is also observed that there is a large jump in the critical wave number between $p = 59$ and $p = 61$. While these results apply when $\delta = 0.01$, we note that for $\delta = 0.03$ the effect of varying the frequency follows a very similar pattern: when $p = 49$ we obtain the critical conditions $a = 0.42$ and $R_c = 370$, while with $p = 75$ we have $a = 0.46$ and $R = 275$.

The analysis summarized here has developed a procedure that has proved capable of explaining mathematically the pivotal role that a small element of high-frequency noise can play in determining the stability of oscillatory flow in a channel. While

Downloaded from https://www.cambridge.org/core. UNIVERSIDAD AUTONOMA METROPOLITANA, on 17 Nov 2026 at 23:50:36, subject to the Cambridge Core terms of use, available at https://www.cambridge.org/core/terms. https://doi.org/10.1017/S1446181126100431

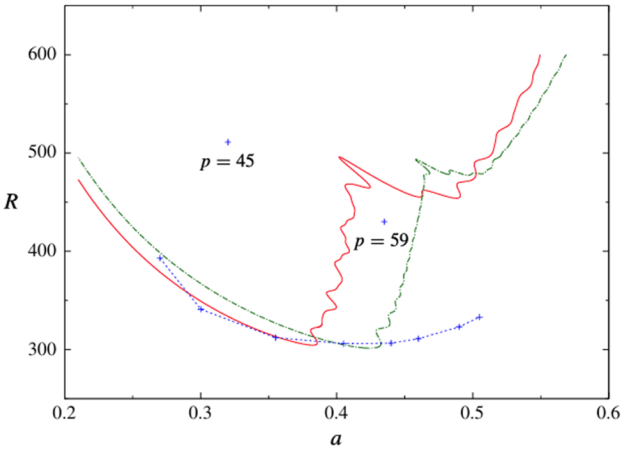


FIGURE 7. The neutral curves for a wide channel $h = 16$ and noise frequencies $p = 69$ (solid curve) and $p = 76$ (dot-dashed curve) with amplitude $\delta = 0.01$. The points denoted by + indicate critical conditions when the perturbation has frequency p as labelled on the graph. The dotted line connects the critical conditions for frequencies $p = 61, 63, 67, 79, 85, 91, 95$ and 105 reading from left to right.

this can be seen theoretically, there is no obvious physical explanation that we can offer for how this could have been anticipated. There have been various attempts made to rationalize the wide discrepancy between the theoretical and experimentally determined values of the transition Reynolds number. Some arguments appeal to nonlinearity, while others suggest that there might be some premature tripping of the flow by wall roughness. Others have proposed scenarios similar to a bypass-type mechanism that can occur in the transition of steady boundary-layer flows. What is added here is convincing proof that even a small element of noise is more than enough to markedly alter the transition characteristics of the flow. Indeed, our results show that it might only be when the noise is reduced to $O(0.01\%)$ that its effect can be ignored, at least for the Stokes layer. Even the most careful experiments claim that the inherent noise component can only be reduced to a value more than an order of magnitude greater than this.

Up to this stage, we have concentrated on the purely temporal response of a Stokes layer to a disturbance and have asked whether a spatially periodic form amplifies or decays. A related question seeks to understand how a perturbation might evolve both in space and time. We consider this aspect next.

5. Spatio-temporal development

The response of disturbances to the Stokes layer in the spatio-temporal $(x, \tau/2\pi)$-plane is best studied following the approach of Ramage and his co-workers that has been detailed in [31, 32, 42]. The basis of this strategy is founded on the idea that disturbances can be decomposed into Fourier components, incorporating the

Downloaded from https://www.cambridge.org/core. UNIVERSIDAD AUTONOMA METROPOLITANA, on 17 Nov 2026 at 23:50:36, subject to the Cambridge Core terms of use, available at https://www.cambridge.org/core/terms. https://doi.org/10.1017/S1446181126100431

discrete wave numbers

$$a = a_q \equiv q\Delta a \quad \text{for } q = 0 \cdots Q.$$

Since the governing system consists of linear equations, and as the base flow is streamwise homogeneous, the various Fourier components evolve independently of each other. This means that the complete spatio-temporal disturbance generated by a localized impulsive wall forcing can be reconstructed by a simple superposition of all Fourier components. For example, the vorticity perturbation can be written as

$$\zeta(x, y, \tau) = \sum_{q=0}^{Q} \zeta_q(y, \tau) \exp(ia_q x);$$

in this formula we have $x = x_q = q\Delta x$ with $\Delta x \equiv 2\pi/((Q + 1)\Delta a)$. The wave number spacing Δa sets the spatial periodicity of the computational domain $2\pi/\Delta a$, and was chosen sufficiently small so as to ensure the accurate resolution of the form of the disturbance; typically $\Delta a = 2.5 \times 10^{-4}$ proved to be adequate for these purposes. Furthermore, the wave number range needs to be wide enough to capture both large- and small-scale behaviours. Practice tests showed that the maximum wave number $a_{\max} = Q\Delta a \approx 0.6$ was adequate. This is somewhat less than might have been anticipated at the outset. However, a larger $a_{\max}$ was not required since wave number components with $a \gtrapprox 0.6$ decay very rapidly indeed.

The governing equations were solved using the numerical scheme developed in [14] based upon a spectral discretisation in the wall-normal y-direction with disturbances expanded in terms of Chebyshev polynomials. The semi-infinite domain $y \in [0, \infty)$ was mapped onto $\xi \in (0, 1]$ using the transformation $\xi = s/(y + s)$; here the stretching parameter s controls the distribution of points across the Stokes layer. The temporal evolution was computed using an implicit-explicit predictor–corrector scheme. The results described below were obtained using the value $s = 4$, 96 Chebyshev polynomials and a time step $\Delta\tau = 0.1/R$ which ensures that there are $O(10^4)$ time steps per period of oscillation.

The typical spatio-temporal evolution of an impulsively generated disturbance is shown in Figure 8. The impulse is applied at $x_f = 0$ and $R = 715$, which corresponds to a marginally unstable case. Figure 8 depicts contours of the logarithm of the wall-vorticity perturbation amplitude in the $(x, \tau/2\pi)$-plane. There is clear evidence of the emergence of a family-tree-like structure. Immediately following the initial impulse when $\tau = 0$, a parent wave packet is formed and this propagates downstream in the positive x-direction. During the first period of oscillation, this parent wave packet produces two child wave packets, which are initiated when there is a sign change in the wall shear stress U'_B. One child packet propagates to the right, which corresponds to a negative-to-positive change in U'_B; the other moves to the left. Each child wave packet subsequently generates two further wave packets over the next period and this process then iterates, thereby generating a repeated branching behaviour that characterizes the formation of a growing family tree.

Downloaded from https://www.cambridge.org/core. UNIVERSIDAD AUTONOMA METROPOLITANA, on 17 Nov 2026 at 23:50:36, subject to the Cambridge Core terms of use, available at https://www.cambridge.org/core/terms. https://doi.org/10.1017/S1446181126100431

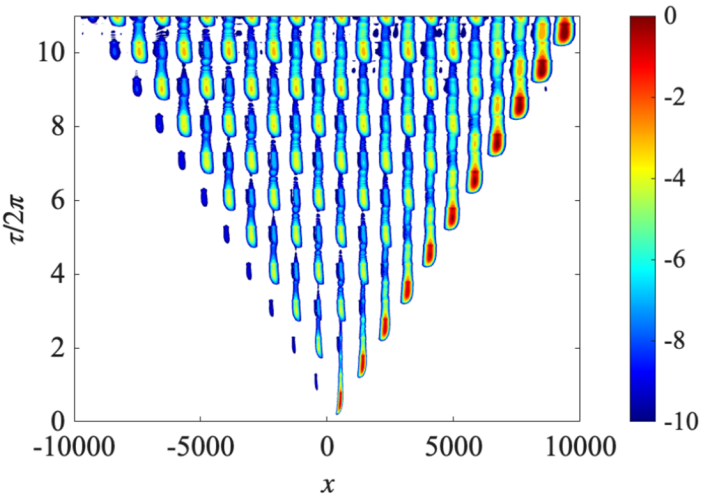


FIGURE 8. A spatio-temporal contour plot of the disturbance quantity $\ln|\zeta|$ at the wall. The calculations correspond to $R = 715$ and a Stokes layer which is impulsively excited at $x_f = 0$.

It is clear from Figure 8 that the disturbance maximum convects along the outermost wave packets on the right-hand side of the tree structure. The corresponding temporal evolution of the maximum wall-vorticity amplitude, $\max_x|\zeta|$, is illustrated in Figure 9(a). From one oscillation period to the next, the disturbance amplitude undergoes a small but sustained increase, which is indicative of the onset of linear instability. An estimate of the growth rate can be derived using the formula

$$\mu_m(\tau) = \frac{1}{2\pi}\ln\left(\frac{\max_x|\zeta(x,0,\tau+2\pi)|}{\max_x|\zeta(x,0,\tau)|}\right),$$

where $\max_x|\zeta|$ is evaluated at the midpoint of each oscillation cycle. The growth rate, as shown in Figure 9(d), approaches a positive constant as τ increases, and this is consistent with the Floquet exponent determined in [5]. Increasing the Reynolds number leads to correspondingly larger growth rates and stronger instability.

The streamwise location of the disturbance maximum $x_{\max}$ is plotted in Figure 9(b). A distinct Λ-spacing emerges between successive wave packets and the disturbance maximum propagates a distance $\Lambda \approx 850$ during each oscillation period. It was shown in [32] that the spacing between adjacent wave packets is proportional to the Reynolds number.

The Stokes layer (2.1) is both time-periodic and anti-periodic in the sense that $U_B(y,\tau+2\pi) = U_B(y,\tau)$ and $U_B(y,\tau+\pi) = -U_B(y,\tau)$. This symmetry structure is reflected in the staggered family-tree disturbance development and its associated temporal response. In particular, the wave-packet formation is approximately symmetric about $x = 0$, except for the outermost packet that contains the disturbance maximum. This symmetry, together with the staggered structure of the packets, leads

Downloaded from https://www.cambridge.org/core. UNIVERSIDAD AUTONOMA METROPOLITANA, on 17 Nov 2026 at 23:50:36, subject to the Cambridge Core terms of use, available at https://www.cambridge.org/core/terms. https://doi.org/10.1017/S1446181126100431

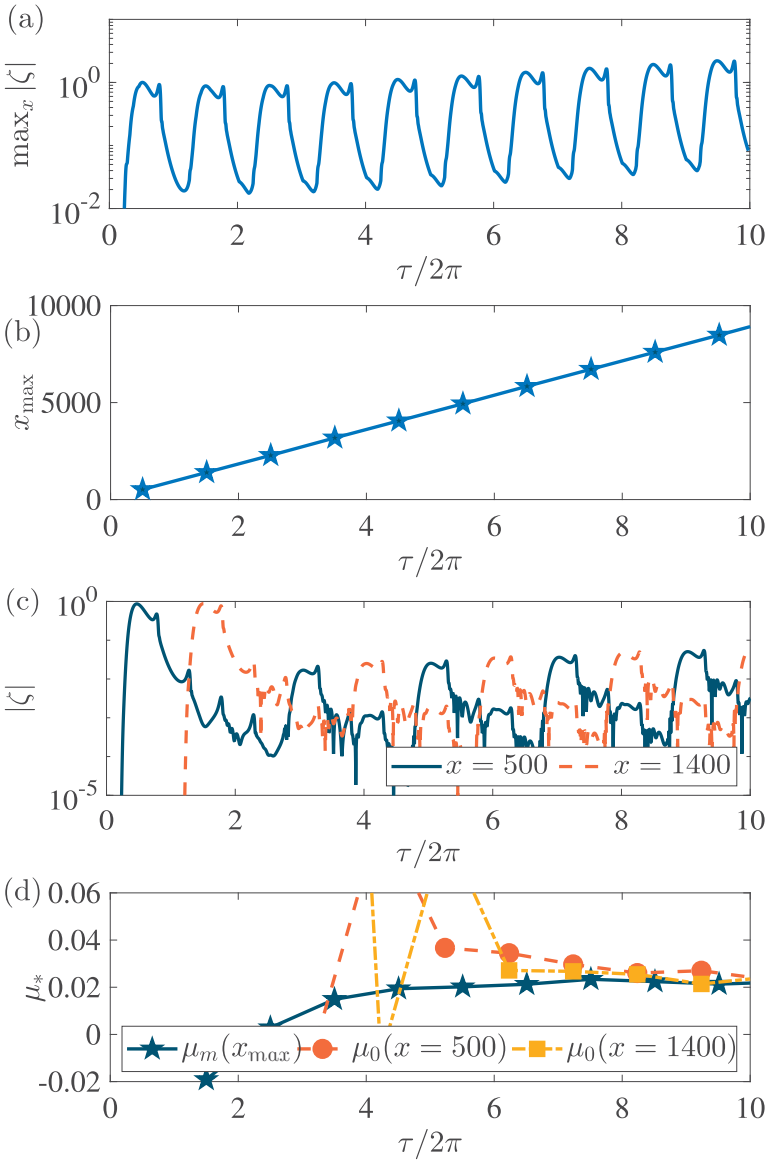


FIGURE 9. The disturbance characteristics of the family-tree structure shown in Figure 8. (a) The temporal evolution of the maximum wall-vorticity perturbation amplitude, $\max_x |\zeta|$. (b) The streamwise location $x_{\max}$ of this maximum measured at the midpoint of each wall cycle (stars). The corresponding line of best fit is shown by the solid line. (c) The temporal evolution of $|\zeta|$ at two locations: $x = 500$ (solid) and $x = 1400$ (dashed). (d) The growth rate μ_m of the disturbance maximum in (a) (solid), and pointwise growth rate, μ_0, at the locations in (c).

Downloaded from https://www.cambridge.org/core. UNIVERSIDAD AUTONOMA METROPOLITANA, on 17 Nov 2026 at 23:50:36, subject to the Cambridge Core terms of use, available at https://www.cambridge.org/core/terms. https://doi.org/10.1017/S1446181126100431

to a separation of 2Λ between packets of commensurate size, thereby leading to an overall spatial periodicity of 2Λ.

The pointwise growth of the disturbance is monitored by fixing a streamwise location and then tracking the temporal development at that location. Figure 9(c) shows the evolution of $|\zeta|$ at the two locations $x = 500$ and $x = 1400$. After an initial transient phase, the peak amplitudes occur alternately between oscillation cycles, which reflects the staggered wave-packet formation. Moreover, the disturbance amplitude increases every two oscillation periods, which demonstrates a sub-harmonic temporal growth with periodicity twice that of the basic state. The pointwise growth rate was calculated using

$$\mu_0(\tau) = \frac{1}{4\pi} \ln\left(\frac{|\zeta(x, 0, \tau + 4\pi)|}{|\zeta(x, 0, \tau)}\right),$$

and the results are illustrated in Figure 9(d). As τ increases, the pointwise growth rates approach the same positive value associated with the disturbance maximum. This observation is consistent with an instability that exhibits absolutely unstable behaviour. Accordingly, we next consider the form of the absolute instability mechanisms that are responsible for the development of the family-tree structure.

5.1. Absolute instability Pretty et al. [29] considered the stability of the Stokes layer using a modified form of the Briggs–Bers [10] method to distinguish between convectively and absolutely unstable behaviour. Convective instability describes a disturbance that grows while propagating in one direction only, whereas absolute instability is characterized by growth at every spatial location. The approach follows [9] for temporally oscillating flows, with Floquet theory used to account for the time-periodicity of the base flow. Given the periodicity properties of the Stokes layer, we can derive symmetry constraints that can help classify the type of instability that develops.

To identify absolute instability, properties were coupled to the cusp-map method [23] in which the streamwise wave number $\alpha \in \mathbb{C}$ is mapped onto the complex Floquet exponent μ-plane. Two types of cusps can arise, and these are associated with Floquet exponents $\mu = \mu_r + ik/2$. If $k = 0$ there is harmonic behaviour, whereas $k = 1$ corresponds to a sub-harmonic structure. Figure 10 demonstrates a cusp structure when $R = 750$ for which $\mu_r = 0.2009$ and $\mu_i = 0$. The cusp occurs at a real-valued wave number α and, since $\mu_r > 0$, symmetry arguments imply pointwise growth and therefore absolute instability. This cusp is associated with $\mu_i = 0$ and corresponds to the tip of a finger-like protrusion along the neutral stability curve and hence harmonic growth. Analogous cusp structures arise for $\mu_i \approx 1/2$ with $\mu_r > 0$, and these are associated with sub-harmonic growth.

When $R = 750$, several cusps with positive real part $\mu_r > 0$ are marked in Figure 11. Four cusps at the tips of fingers ($\mu_i = 0$) are shown by the red circular markers and three cusps with $\mu_i \approx 1/2$ are located about the mid-points between adjacent protrusions. The pointwise growth is therefore characterized by a combination of harmonic and

Downloaded from https://www.cambridge.org/core. UNIVERSIDAD AUTONOMA METROPOLITANA, on 17 Nov 2026 at 23:50:36, subject to the Cambridge Core terms of use, available at https://www.cambridge.org/core/terms. https://doi.org/10.1017/S1446181126100431

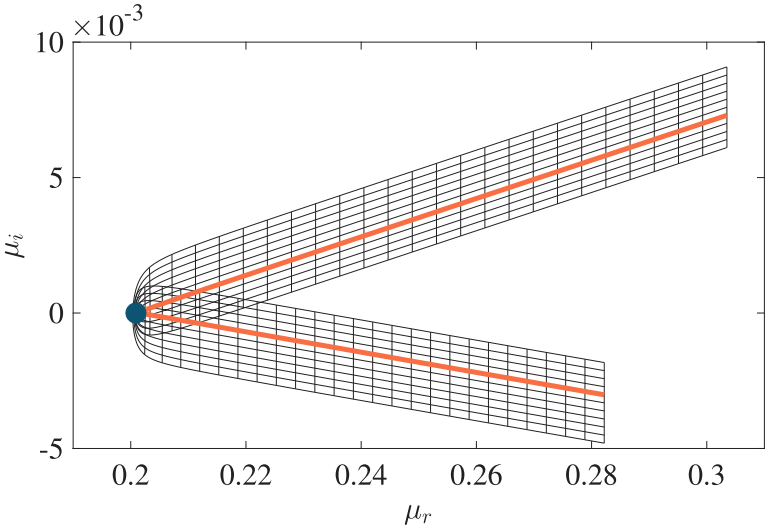


FIGURE 10. Cusp formation in the complex μ-plane when $R = 750$. This solution corresponds to $\mu_i = 0$ and the tip of a finger protrusion in Figure 11.

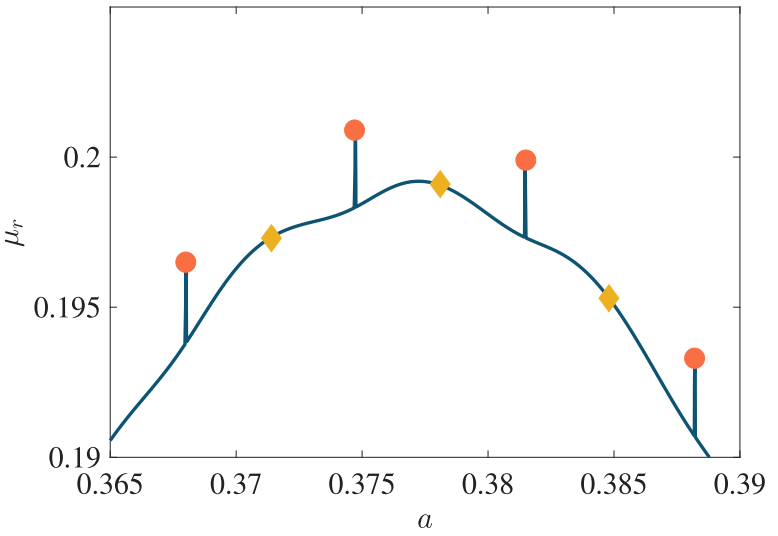


FIGURE 11. The Floquet growth rate μ_r as a function of wave number a when $R = 750$. The red circle and yellow diamond markers highlight locations matched to absolutely unstable harmonic ($\mu_i = 0$) and sub-harmonic modes ($\mu_i = 1/2$), respectively.

sub-harmonic absolutely unstable modes. These features extend to other Reynolds numbers, including the critical value $R_c \approx 707.84$, where a stationary disturbance first appears along a $\mu_i = 0$ finger. This proves that the onset of instability coincides with the onset of absolute instability.

Downloaded from https://www.cambridge.org/core. UNIVERSIDAD AUTONOMA METROPOLITANA, on 17 Nov 2026 at 23:50:36, subject to the Cambridge Core terms of use, available at https://www.cambridge.org/core/terms. https://doi.org/10.1017/S1446181126100431

Further work in this direction by Ramage et al. [32] examined the effect of introducing a high-frequency component of noise into the basic flow. It will be recalled that [41] had previously shown that even a small noise element proportional to $\cos(p\tau)$ is sufficient to significantly reduce the critical Reynolds number for linear instability. For small amplitudes, the disturbance retains the family-tree structure and sub-harmonic growth, but a distinction needs to be drawn on whether p is even or odd. When $p/2 \in \mathbb{N}$, an additional spatial asymmetry arises owing to a breakdown of the anti-periodicity of the oscillatory basic state, since the relation $U_B(y, \tau + \pi) = -U_B(y, \tau)$ no longer holds. The symmetry between positive and negative directions that characterizes the unmodified Stokes layer is then lost. As the amplitude of the high-frequency harmonic is increased, the family-tree formation is gradually modified and eventually becomes a single wave packet that alternates in space between successive cycles. Concurrently, the sub-harmonic behaviour observed in the unmodified Stokes layer is replaced by oscillations at the fundamental period of the modified base state. The overall effect is that absolutely unstable behaviour becomes evident at earlier times than in the canonical Stokes layer.

5.2. Skewed flows The basic Stokes layer can be extended to include both acceleration and velocity skewness. This introduces asymmetry into the periodic base flow and the resulting profile is thought to be a good model for motions seen in coastal dynamics where wave propagation is characterized by skewness in the wave depth, wave height and wave period. The velocity skewness generates a wave characterized by a narrow, sharp crest together with a broad, flat trough, while acceleration skewness produces wave asymmetry.

The linear stability of acceleration-skewed and velocity-skewed flows has been investigated in [35, 36], respectively. Acceleration skewness tends to destabilize the Stokes layer and reduces the critical Reynolds number, while velocity skewness has the opposite effect. Further insight into the effect of skewness on linear instability is provided by the impulse response of disturbances in the spatio-temporal plane, as described in [43]. Figure 12 illustrates the typical behaviour observed in both acceleration-skewed and velocity-skewed flows for conditions matched to linear instability. While the overall structure is similar to the family-tree behaviour observed in the symmetric Stokes layer (see Figure 8), skewness introduces a marked asymmetry in the spatial development. The disturbance maximum again convects along the rightmost branch of the structure, but wave packets propagating to the left decay and ultimately dissipate. The consequence is that the characteristic sub-harmonic growth associated with the Stokes layer is lost. This behaviour arises because acceleration- and velocity-skewed flows are no longer anti-periodic, unlike the classical Stokes layer. As a result, the onset of linear instability in skewed flows corresponds to convective instability rather than the absolute instability observed for the Stokes layer. It is only at a much higher Reynolds number that sub-harmonic growth re-emerges and absolute instability sets in.

Downloaded from https://www.cambridge.org/core. UNIVERSIDAD AUTONOMA METROPOLITANA, on 17 Nov 2026 at 23:50:36, subject to the Cambridge Core terms of use, available at https://www.cambridge.org/core/terms. https://doi.org/10.1017/S1446181126100431

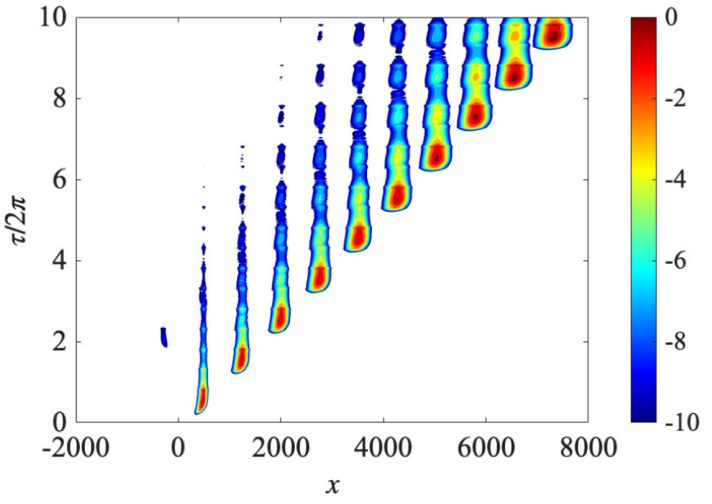


FIGURE 12. A spatio-temporal contour plot of the linear disturbance $\ln|\zeta|$ in an acceleration-skewed Stokes layer. Here $R = 635$ and motion is impulsively excited at $x_f = 0$.

6. Discussion

In this work, we have described some of the progress that has been made in our understanding of the stability of the classical plane Stokes layer. This motion, which constitutes one of the few exact solutions of the ubiquitous Navier–Stokes equations, has proved surprisingly resistant to rigorous stability analysis. We have deliberately focused on the Stokes layer in its simplest form, although several generalisations have also been examined. These include the addition of suction/injection [19], magnetic fields [40] and extensions to various non-Newtonian flows. In this regard, we should mention that studies have been directed to power law [30], viscoplastic [3], viscoelastic [26] and discontinuously shear-thickening fluids [21].

Further studies have been directed to enhance our understanding of the receptivity of Stokes layers to wall roughness [8, 45, 46]. More recently, investigations of oscillatory and pulsatile flows have focused on linear and nonlinear dynamics of the Floquet modal instability [27] and nonmodal transient behaviour [4, 28, 49]. Contemporary work has examined the role that edge states, which are linked to streak–wave–roll interactions, may play in controlling and sustaining Stokes layer flows.

In conclusion, we reiterate that the work described herein is restricted to linear theory and is applied only to the most straightforward of plane Stokes layers. It is highly likely that similar results would transfer across to other time-periodic boundary-layer flows. If this is indeed the case, the implication for practical studies could be significant. The wide discrepancy between the analytical predictions and the practical measurements of stability thresholds is unfortunate but is also potentially

Downloaded from https://www.cambridge.org/core. UNIVERSIDAD AUTONOMA METROPOLITANA, on 17 Nov 2026 at 23:50:36, subject to the Cambridge Core terms of use, available at https://www.cambridge.org/core/terms. https://doi.org/10.1017/S1446181126100431

difficult to avoid. Small components of high-frequency noise appear to be enough to change the stability characteristics quite markedly, and even the most careful experiments are unable to be conducted with sufficient precision to circumvent this.

Acknowledgements

We are indebted to Peter Blennerhassett, who collaborated in much of the work described here. Peter retired from UNSW and we have subsequently lost touch; otherwise, we would have certainly asked him to contribute to this article. If any reader knows of his whereabouts, we would be delighted to know. We also gratefully acknowledge Christopher Davies and Alexander Pretty for their substantial contributions to the work on the spatio-temporal development.

The referees are thanked for their very helpful comments which have led to a much improved paper.

References

[1] R. Akhaven, R. D. Kamm and A. H. Shapiro, "An investigation of transition to turbulence in bounded oscillatory flows. Part 1. Experiments", *J. Fluid Mech.* **225** (1991) 395–422; doi:10.1017/S0022112091002100.

[2] R. Akhaven, R. D. Kamm and A. H. Shapiro, "An investigation of transition to turbulence in bounded oscillatory flows. Part 2. Numerical simulations", *J. Fluid Mech.* **225** (1991) 423–444; doi:10.1017/S0022112091002112.

[3] N. J. Balmforth, Y. Forterre and O. Pouliquen, "The viscoplastic Stokes layer", *J. Non-Newton. Fluid Mech.* **158** (1) (2009) 46–53; doi:10.1016/j.jnnfm.2008.07.011.

[4] D. Biau, "Transient growth of perturbations in Stokes oscillatory flows", *J. Fluid Mech.* **794** (2016) Article ID: R4; doi:10.1017/jfm.2016.210.

[5] P. J. Blennerhassett and A. P. Bassom, "The linear stability of flat Stokes layers", *J. Fluid Mech.* **464** (2002) 393–410; doi:10.1017/S0022112002001052.

[6] P. J. Blennerhassett and A. P. Bassom, "The linear stability of high-frequency oscillatory flow in a channel", *J. Fluid Mech.* **556** (2006) 1–25; doi:10.1017/S0022112006009141.

[7] P. J. Blennerhassett and A. P. Bassom, "A note on the linear stability of a two-dimensional Stokes layer", *Quart. J. Mech. Appl. Math.* **60** (2007) 391–396; doi:10.1093/qjmam/hbm014.

[8] P. Blondeaux and G. Vittori, "Wall imperfections as a triggering mechanism for Stokes-layer transition", *J. Fluid Mech.* **264** (1994) 107–135; doi:10.1017/S0022112094000601.

[9] L. Brevdo and T. J. Bridges, "Absolute and convective instabilities of temporally oscillating flows", *Z. Angew. Math. Phys.* **48** (1997) 290–309; doi:10.1007/PL00001477.

[10] R. J. Briggs, *Electron-Stream Interaction with Plasmas* (MIT Press, Cambridge, MA, 1964).

[11] M. Clamen and P. Minton, "An experimental investigation of flow in an oscillating pipe", *J. Fluid Mech.* **81** (1977) 421–431; doi:10.1017/S0022112077002146.

[12] S. J. Cowley, "High frequency Rayleigh instability analysis of Stokes layers", in: *Stability of Time-Dependent and Spatially Varying Flows* (eds D. L. Dwoyer and M. Y. Hussaini) (Springer, New York, 1987) 261–275; doi:10.1007/978-1-4612-4724-1_14.

[13] W. O. Criminale, T. L. Jackson and R. D. Joslin, *Theory and Computation of Hydrodynamic Stability*, *Cambridge Monographs on Mechanics* (Cambridge University Press, Cambridge, 2003).

[14] C. Davies and P. W. Carpenter, "A novel velocity-vorticity formulation of the Navier–Stokes equations with applications to boundary layer disturbance evolution", *J. Comput. Phys.* **172** (2001), 119–165; doi:10.1016/S00219991(01)96817–2.

[15] M. O. De Souza, "Instabilities of rotating and unsteady flows", Ph.D. Thesis, Cambridge University, 1998.

Downloaded from https://www.cambridge.org/core. UNIVERSIDAD AUTONOMA METROPOLITANA, on 17 Nov 2026 at 23:50:36, subject to the Cambridge Core terms of use, available at https://www.cambridge.org/core/terms. https://doi.org/10.1017/S1446181126100431

[16] P. G. Drazin and W. H. Reid. *Hydrodynamic Stability* (Cambridge University Press, Cambridge, 1984).
[17] D. M. Eckmann and J. B. Grotberg, "Experiments on transition to turbulence in oscillatory pipe flow", *J. Fluid Mech.* **222** (1991) 329–350; doi: 10.1017/S002211209100112X.
[18] B. Fornberg, *A Practical Guide to Pseudospectral Methods* (Cambridge University Press, Cambridge, 1996), doi:10.1017/CBO9780511626357.
[19] P. Gau and X. Y. Lu, "Effect of wall suction/blowing on the linear stability of flat Stokes layers", *J. Fluid Mech.* **551** (2006) 303–308; doi: 10.1017/S002211200500782X.
[20] P. Hall, "The linear stability of flat Stokes layers", *Proc. Roy. Soc. London Sect. A* **359** (1978), 151–166; doi:10.1098/rspa.1978.0037.
[21] D. R. Hewitt and N.J. Balmforth, "Stokes layers in complex fluids", *J. Non-Newton. Fluid Mech.* **334** (2024) Article ID: 105328; doi:10.1016/j.jnnfm.2024.105342.
[22] M. Hino, M. Sawamoto and S. Takasu, "Experiments on transition to turbulence in an oscillatory pipe flow", *J. Fluid Mech.* **75** (1976) 193–207; doi:10.1017/S0022112076000177.
[23] K. Kupfer, A. Bers and A. K. Ram, "The cusp map in the complex-frequency plane for absolute instabilities", *Phys. Fluids* **30** (1987) 3075–3082; doi:10.1063/1.866483.
[24] J. Luo and X. Wu, "On the linear instability of a finite Stokes layer: Instantaneous versus Floquet modes", *Phys. Fluids* **22** (2010), 054106; doi:10.1063/1.3407665.
[25] H. J. Obremski and M. V. Morkovin, "Application of a quasi-steady stability model to periodic boundary-layer flows", *AIAA J.* **7** (1969) 1298–1301; doi:10.2514/3.5337.
[26] J. Ortín. "Stokes layers in oscillatory flows of viscoelastic fluids". *Philos. Trans. Roy. Soc. London A* **378** (2174) (2020) Article ID: 20190521; doi:10.1098/rsta.2019.0521.
[27] B. Pier and P. Schmid, "Linear and nonlinear dynamics of pulsatile channel flow", *J. Fluid Mech.* **815** (2017) 435–480; doi:10.1017/jfm.2017.58.
[28] B. Pier and P. Schmid, "Optimal energy growth in pulsatile channel and pipe flows", *J. Fluid Mech.* **926** (2021) Article ID: A11; doi:10.1017/jfm.2021.702.
[29] A. Pretty, C. Davies and C. Thomas, "Onset of absolutely unstable behaviour in the Stokes layer: a Floquet approach to the Briggs method", *J. Fluid Mech.* **928** (2021) Article ID: A23; doi:10.1017/jfm.2021.824.
[30] D. Pritchard, C. R. McArdle and S. K. Wilson, "The Stokes boundary layer for a power-law fluid", *J. Non-Newton. Fluid Mech.* **166** (12) (2011) 745–753; doi:10.1016/j.jnnfm.2011.04.011.
[31] A. Ramage, "Linear disturbance evolution in the semi-infinite Stokes layer and related flows", Ph.D. Thesis, School of Mathematics, Cardiff University, 2017.
[32] A. Ramage, C. Davies, C. Thomas and M. Togneri, "Numerical simulation of the spatiotemporal development of linear disturbances in Stokes layers: Absolute instability and the effects of high-frequency harmonics", *Phys. Rev. Fluids* **5** (2020) Article ID: 103901; doi:10.1103/PhysRevFluids.5.103901.
[33] G. Seminara and P. Hall, "Centrifugal stability of a Stokes layer", *Proc. Roy. Soc. London Sect. A* **350** (1976) 299–316; doi:10.1098/rspa.1976.0109.
[34] H. B. Squire, "On the stability for three-dimensional disturbances of viscous fluid flow between parallel walls", *Proc. Roy. Soc. London Sect. A* **142** (1933) 621–628; doi:10.1098/rspa.1933.0193.
[35] C. Thomas, "The linear stability of an acceleration-skewed oscillatory Stokes layer", *J. Fluid Mech.* **895** (2020) Article ID: A27; doi:10.1017/jfm.2020.345.
[36] C. Thomas, "Effects of velocity skewness on the linear stability of the oscillatory Stokes layer", *Phys. Fluids* **33** (2021) Article ID: 034104; doi:10.1063/5.0043146.
[37] C. Thomas, A. P. Bassom and P. J. Blennerhassett, "The linear stability of oscillating pipe flow", *Phys. Fluids* **24** (2012) Article ID: 014106; doi:10.1063/1.3673603.
[38] C. Thomas, A. P. Bassom, P. J. Blennerhassett and C. Davies, "Direct numerical simulations of small disturbances in the classical Stokes layer", *J. Eng. Math.* **68** (2010) 327–338; doi:10.1007/s10665–010–9381–0.
[39] C. Thomas, A. P. Bassom, P. J. Blennerhassett and C. Davies, "The linear stability of oscillatory Poiseuille flow in channels and pipes", *Proc. Roy. Soc. London Sect. A* **467** (2011) 2643–2662; doi:10.1098/rspa.2011.0022.

Downloaded from https://www.cambridge.org/core. UNIVERSIDAD AUTONOMA METROPOLITANA, on 17 Nov 2026 at 23:50:36, subject to the Cambridge Core terms of use, available at https://www.cambridge.org/core/terms. https://doi.org/10.1017/S1446181126100431

[40] C. Thomas, A. P. Bassom and C. Davies. "The linear stability of a Stokes layer with an imposed axial magnetic field". *J. Fluid Mech.* **662** (2010) 320–328; doi:10.1017/S0022112010004210.

[41] C. Thomas, P. J. Blennerhassett, A. P. Bassom and C. Davies, "The linear stability of a Stokes layer subjected to high frequency perturbations". *J. Fluid Mech.* **764** (2015) 193–218; doi: 10.1017/S002211201400612X.

[42] C. Thomas, C. Davies, A. P. Bassom and P. J. Blennerhassett, "Evolution of disturbance wavepackets in an oscillatory Stokes layer", *J. Fluid Mech.* **752** (2014) 543–571; doi:10.1017/S0022112014002613.

[43] C. Thomas and A. Pretty, "Impulse response of linear disturbances in a skewed Stokes layer", *Phys. Fluids* **37** (2025) Article ID: 014107; doi:10.1063/5.0249527.

[44] L. N. Trefethen, *Spectral Methods in MATLAB* (SIAM, Philadelphia, PA, 2000), doi:10.1137/1.9780898719598.

[45] R. Verzicco and G. Vittori, "Direct simulation of transition in Stokes boundary layers", *Phys. Fluids* **8** (1996) 1341–1343; doi:10.1063/1.868940.

[46] G. Vittori and R. Verzicco, "Direct simulation of transition in an oscillatory boundary layer", *J. Fluid Mech.* **371** (1998) 207–232; doi: 10.1017/S002211209800282X.

[47] C. von Kerczek and S. H. Davis, "Linear stability theory of oscillatory Stokes layers". *J. Fluid Mech.* **62** (1974) 753–773; doi:10.1017/S0022112074000929.

[48] X. S. Wu and S. J. Cowley, "On the nonlinear evolution of instability modes in unsteady shear layers – the Stokes layer as a paradigm", *Quart. J. Mech. Appl. Math.* **48** (1995) 159–188; doi:10.1093/qjmam/48.2.159.

[49] D. Xu, B. Song and M. Avila, "Non-modal transient growth of disturbances in pulsatile and oscillatory pipe flows", *J. Fluid Mech.* **905** (2021) Article ID: R5; doi:10.1017/jfm.2020.940.

Downloaded from https://www.cambridge.org/core. UNIVERSIDAD AUTONOMA METROPOLITANA, on 17 Nov 2026 at 23:50:36, subject to the Cambridge Core terms of use, available at https://www.cambridge.org/core/terms. https://doi.org/10.1017/S1446181126100431